Flexible Curcumin-Loaded Zn-MOF Hydrogel for Long-Term Drug Release and Antibacterial Activities

Li Jiaxin , Yan Yachao , Chen Yingzhi * , Fang Qinglin , Muhammad Irfan Hussain , And Wang Lu-Ning *

Posted Date: 12 June 2023

doi: 10.20944/preprints202306.0503.v2

Keywords: Curcumin; MOF; Sodium Alginate Hydrogel; Drug Release; Antibacterial Activity

Article

Flexible Curcumin-Loaded Zn-MOF Hydrogel for Long-Term Drug Release and Antibacterial Activities

Li Jiaxin [1,†], Yan Yachao [1,†], Chen Yingzhi [1,2,*], Fang Qinglin [1], Muhammad Irfan Hussain [1] and Wang Lu-Ning [1,2,*]

[1] School of Materials Science and Engineering, University of Science and Technology Beijing, Beijing 100083, China
[2] Shunde Graduate School of University of Science and Technology Beijing, Foshan, Guangdong 528399, China
* Correspondence: chenyingzhi@ustb.edu.cn (C.Y.); luning.wang@ustb.edu.cn (W.L)
† These authors contributed equally to this work.

Abstract: Management of chronic inflammation and wounds has always been a key issue in the pharmaceutical and healthcare sector. Curcumin (CCM) is an active ingredient extracted from turmeric rhizomes that has antioxidant, anti-inflammatory, and antibacterial activities, thus showing significant effectiveness toward wound healing. However, its shortcomings such as poor water solubility, poor chemical stability and fast metabolic rate limit its bioavailability and long-term use. In this context, hydrogels appear to be a versatile matrix for carrying and stabilizing drugs due to the biomimetic structure, soft porous microarchitecture, and pleasant biomechanical properties. The drug loading/releasing efficiencies can also be controlled by use of highly crystalline and porous metal organic frameworks (MOFs). Here, a flexible hydrogel composed of sodium alginate (SA) matrix and CCM-loaded MOFs was constructed for long-term drug release and antibacterial activity. The morphology and physicochemical properties of composite hydrogels were analyzed by scanning electron microscopy (SEM), Fourier transform infrared spectroscopy (FT-IR), X-ray diffraction (XRD), ultraviolet visible spectroscopy (UV-Vis), Raman spectroscopy and mechanical property tests. The results showed that the composite hydrogel was highly twistable and bendable to mechanically comply with human skin. The as-prepared hydrogel could capture efficient CCM for slow drug release as well as effective killing of bacteria. Therefore, such composite hydrogel is expected to provide a new management system for chronic wound dressings.

Keywords: curcumin; MOF; sodium alginate hydrogel; drug release; antibacterial activity

1. Introduction

Chronic wounds and the accompanying persistent bacterial inflammation have always been a vital challenge in clinical treatment. For the treatment of wounds, curcumin (CCM) is highly recognized in benefitting the human health[1]. It is a natural lipophilic polyphenol and natural antioxidant compound that has been widely used as a food additive, food coloring[2] and flavoring agent[3] in the past decades, and in recent years researches have revealed the pleiotropic nature of the biological effects of this molecule. Many researches have clarified its antioxidant, anti-inflammatory, and antibacterial activities which are beneficial for wound healing[4]. However, poor water solubility (under acidic and neutral conditions), chemical instability (especially under neutral and alkaline conditions), rapid metabolic rate limited bioavailability and delivery efficiency severely affect its application on wound healing[5]. In this regard, nanotechnology-based delivery systems (encapsulating the drug into specific nanocarriers) are considered as a promising technology for circumventing these obstacles.

So far, various drug delivery platforms have been developed, mainly including polymeric nanoparticles[6], carbon-based nanostructures, lipid-based nanoparticles[7] and inorganic nanostructures[8]. Among them, carbon-based nanostructures display high surface area,

functionalization versatility and drug loading capacity for drug delivery[9]. Biomolecules, such as lipids or proteins, are good choices as biocompatible platforms[10]; Inorganic or organic nanoparticles are appealing for their altered pharmacokinetics and biodistribution profiles, sometimes presenting unique photonic/thermal/electronic/magnetic effects in guiding the accumulation or release of drugs[11,12]. To combine the merits of loading efficiency, tunability and biocompatibility, metal organic frameworks (MOFs) stand out as promising antibacterial platforms. MOFs are a class of highly crystalline and nanoporous materials that can be built from various metal ions or metal clusters and organic linkers for tunable chemical and topological structures[13]. Recently, increasing use of MOFs has been made in drug storage and release for their combined properties of high adsorption capacity, tunable host-guest interaction and release efficiency, biocompatibility and nontoxicity[14].

To be properly used as wound dressing, it should also be able to fill wound spaces, and provide mechanical stability as well as good penetrability to water vapor and metabolites. Hydrogels with three-dimensional (3D) hydrophilic polymeric structures can meet these requirements[15], by mimicking the native extracellular matrix (flexible and stable shape, strong plasticity, and not stick to the wound), and creating a moist microenvironment for wound[16]. At the same time, hydrogels can host various bioactive ingredients[17], and their high porosity and controllable crosslinking allow them to be delivered in a suitable manner for accelerating wound healing[18]. The water absorption and penetrability of hydrogels arises from their flexible polymer network with many hydrophilic groups[19] (*e.g.*, R-COOH, R-$CONH_2$, R-NH_2, R-OH, R-SO_3H). These functional groups in hydrogels make it easy to adsorb metal ions via binding with various oxygen, nitrogen, or sulfur -containing functional groups [20]. This also provides the anchoring sites for the nucleation and growth of MOFs, highlighting the rational design of efficient wound dressing system.

In this study, CCM ligands and Zn^{2+} centered MOF (CCM@ZIF-8) with similar structure to ZIF-8 was prepared onto sodium alginate (SA) hydrogel to improve the stability and administration efficiency of CCM, affording controlled release of CCM, and improve bioavailability. By changing the amount of hosted CCM, the composite hydrogel displayed controlled antibacterial and anti-inflammatory effects. The composite hydrogel also exhibited reasonable flexibility that could be twisted and bended on human skin, promising for the use of wound dressing. Such system makes full use of the performance advantages and structural characteristics of each conventional single component, circumventing the shortcomings of CCM, traditional dressings and MOFs in biomedical application, thus providing a rational design guideline for antibacterial CCM-based platform for wound healing.

2. Results and Discussion

2.1. Characterization of CCM@ZIF-8@SA composite hydrogels

Zn^{2+} was used as the cross-linking agent for the preparation of flexible sodium SA hydrogels, and the surficial Zn^{2+} on the as-prepared hydrogel could also work as metal coordinated center to simultaneously connect with 2-Methylimidazole (2-mIM) ligand and CCM, leading to the formation of CCM-loaded Zn-MOF hydrogel (CCM@ZIF-8@SA), as shown in Figure 1a. With increasing the enrolled CCM amount (1.0, 3.0 and 5.0 mg), three kinds of composite hydrogels are obtained, that was 1CCM@ZIF-8@SA, 3CCM@ZIF-8@SA and 5CCM@ZIF-8@SA accordingly. The optical and the scanning electron microscopy (SEM) images of the as-prepared SA, ZIF-8@SA and 1/3/5CCM@ZIF-8@SA were depicted in Figure 1. From the optical picture, it could be seen that the SA hydrogel after Zn^{2+} crosslinking was transparent (Figure 1b), and after loading ZIF-8 particles, the sample changed from transparent to white (Figure 1c). When CCM was added together with the coordination ligand, the sample color turned orange and gradually deepened as the CCM amount increased (Figure 1d-f). As shown in the SEM image (Figure 1g-k), they all had a porous sponge structure, which would contribute to water retention/penetration and sustained drug release inside the hydrogel. As shown in the magnified insets in Figure 1g-h, the surface of SA hydrogel was smooth, while coordination of Zn^{2+} with 2-mIM gave rise to regular dodecahedral ZIF-8 particles homogeneously dispersed on SA (ZIF-8@SA). From Figure 1i, it could be seen the small dosage of CCM did not change the surface sate

a bit, but when the added CCM amount was increased to 3mg, most of the regular dodecahedral structure was replaced by a sheet structure (Figure 1j), meaning the CCM could work as the regulator in the coordination reaction and even as another ligand to coordinate with Zn^{2+} , thus rebuilding the MOF structure[21, 22]; With CCM increased to 5 mg (inset in Figure 1k), the surface dodecahedral structures were totally changed to lamellar structures, verifying the similar role of CCM as ligands. The lamellar structures were promised to serve as effective channels for drug release.

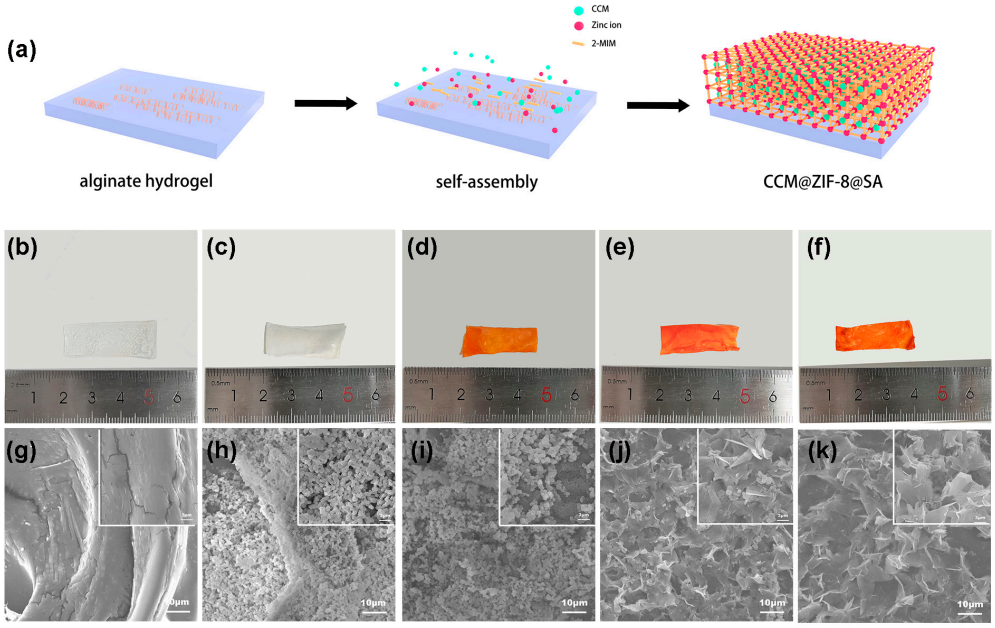

Figure 1. (a) Schematic diagram of the synthesis of a hydrogel, Optical photo of SA (b), ZIF-8@SA (c), 1CCM@ZIF-8@SA (d), 3CCM@ZIF-8@SA (e), 5CCM@ZIF-8@SA (f), SEM images of SA (g), ZIF-8 @SA (h), 1CCM@ZIF-8@SA (i), 3CCM@ZIF-8@SA (j), 5CCM@ZIF-8@SA (k).

From the X-ray diffraction (XRD) patterns (Figure 2a), it could be seen ZIF-8 had characteristic diffraction peaks at 7.39, 10.45, 12.84 and 16.51°, which corresponded to the (110), (200), (211) and (222) planes, respectively[23]. These typical peaks appeared in the ZIF-8@SA and still remained in 5CCM@ZIF-8@SA (containing the most CCM) samples, indicating that ZIF-8 crystals were successfully formed onto the hydrogel[24], but also the participation of CCM did not affect the packing of ZIF-8.The Fourier transform infrared spectroscopy (FT-IR) spectra were shown in Figure 2b. Characteristic peaks of CCM and ZIF-8 were present in 1/3/5CCM@ZIF-8@SA, evidencing the successful incorporation of CCM into ZIF-8. Compared with pure CCM, the stretched peak of the phenol group in 1/3/5CCM@ZIF-8@SA showed a blue shift from the original 3490 to 3435 cm^{-1}, which was probably attributed to the strong interaction between CCM and Zn^{2+}[25]. To confirm the presence of CCM into ZIF-8, the UV−vis absorption analysis was conducted (Figure 2c). As displayed, CCM had a characteristic absorption band at 427 nm; After hosted, a strong but wide absorption peak (at 440 nm) was observed in 1/3/5CCM@ZIF-8@SA, meaning a marked red shift of about 13 nm relative to the pure CCM. This further revealed the strong interaction between CCM and Zn^{2+} either in ZIF-8 or the hydrogel, which decreased the band gap between $\pi-\pi^*$[26] electronic transition of CCM. It is supposed that CCM contains highly conjugated 1,3-diketones moiety (1, 3-diketones and two enols) in the tautomer, which could be connected with Zn^{2+} to form porous skeleton compounds with stable structure. In the Raman spectra (Figure 2d), no obvious bond was found in SA; ZIF-8@SA showed the characteristic bonds of ZIF-8 at 286 cm^{-1} (Zn-N vibrations in the ZnN_4 tetrahedron)[27], 1123 cm^{-1} (C-N stretching), and 1461 cm^{-1} (C-H)[28], indicating the successful loading of ZIF-8 onto SA; The extrafaceted bending vibration of the imidazole ring at 694 cm^{-1} was assigned to Zn-N vibrations[29]. These distinct Raman bands of CCM were also observed in 1/3/5CCM@ZIF-8@SA, further confirming the incorporation of CCM[30].

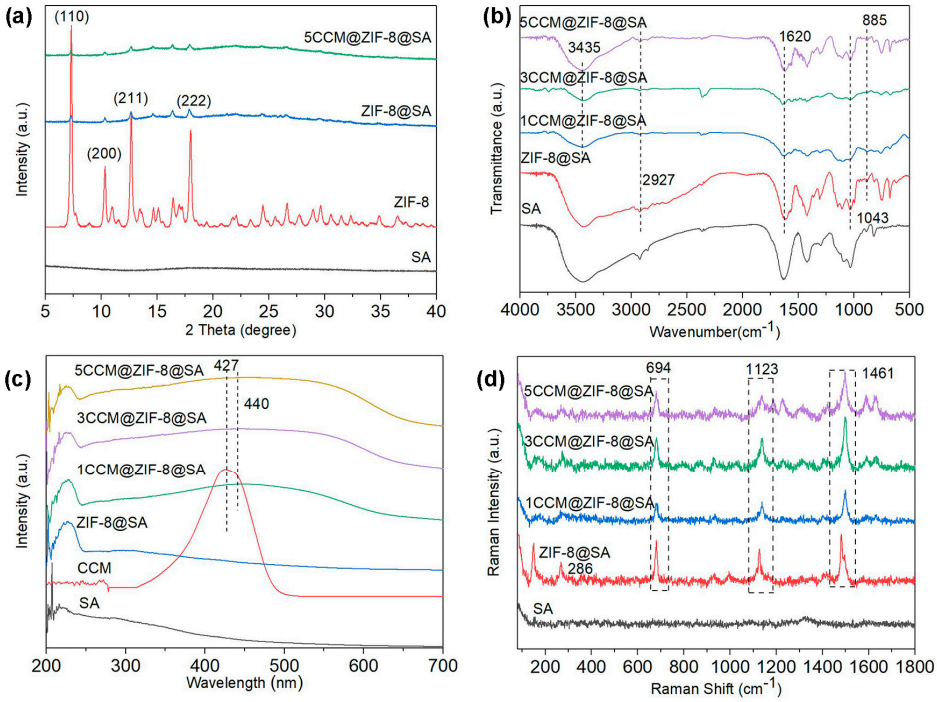

Figure 2. (a) XRD spectra of SA, ZIF-8, ZIF-8@SA and 5CCM@ZIF-8@SA, (b) FTIR spectra of CCM, ZIF-8@SA, 1/3/5CCM@ZIF-8@SA, (c) UV-Vis absorption spectra of SA, ZIF-8@SA, 1/3/5CCM@ZIF-8@SA, (d) Raman spectra of SA, ZIF-8@SA, 1/3/5CCM@ZIF-8@SA.

The mechanical properties of composite hydrogels were then tested. As shown in Figure 3a, the tensile strength increased with the addition of CCM and ZIF-8. Compared with the SA hydrogel (7.66 MPa), the ultimate tensile strengths of the ZIF-8@SA and 5CCM@ZIF-8@SA were 10.67 MPa and 11.95 MPa, respectively. This might be attributed to the formation of supplementary chemical cross-linking (*i.e.*, coordination bond, hydrogen bond) between ZIF-8 and SA[31, 32]. To verify its flexibility, bending and twisting tests were conducted on 5CCM@ZIF-8@SA samples. As shown in Figure 3b, the 5CCM@ZIF-8@SA sample could endure a large degree of distortion and still maintained the original shape after twisting. When the hydrogel was adhered to the finger joints and with bending (Figure 3c), the sample did not break after bending by 120°, 90° and 60°. These results indicated its good toughness and flexibility, promising for its use as the wound dressing.

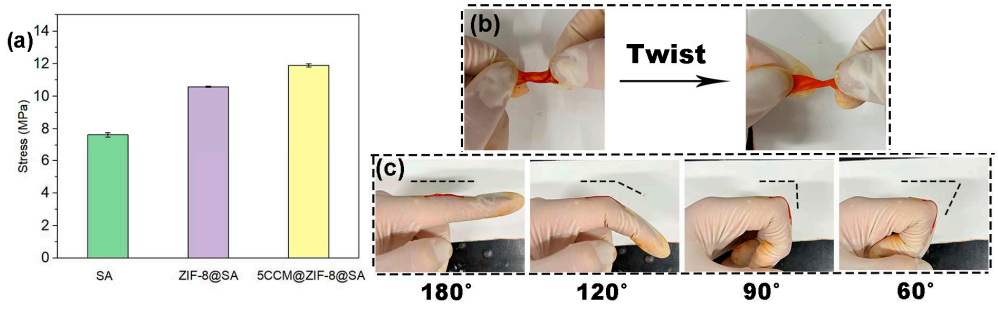

Figure 3. (a) Stress-strain image of SA, ZIF-8@SA and 5CCM@ZIF-8@SA, (b) twisting behavior of 5CCM@ZIF-8@SA, (c) bending behavior of 5CCM@ZIF-8@SA.

2.2. Drug release behavior of CCM@ZIF-8@SA composite hydrogel

According to the wavelength scans of different concentrations of CCM ethanol solution and the standard curve of CCM, a linear fit yielded the relationship between CCM concentration and absorbance values as y=0.14617x+0.02948 with a correlation coefficient R^2 = 0.99562 (Figure 4a,b). The

cumulative concentration of CCM released from the three samples of 1CCM@ZIF-8@SA, 3CCM@ZIF-8@SA and 5CCM@ZIF-8@SA were shown in Figure 4c. The release of CCM increased rapidly in the first 4 h, after which the rising trend of release gradually slowed down and finally approached a steady state. This was because CCM was encapsulated inside the small pores of ZIF-8 framework. At the initial stage of release, the CCM on the surface and near the pores diffused into the solution (related to the fast swelling capacity of the sample surface)[33], while most of the CCM inside remained encapsulated inside the particles[34]. Therefore, the release of CCM inside the granules would be slow, and a long-term release behavior could be achieved. It followed similar release pattern for three samples. Compared with the relatively rapid release for 1CCM@ZIF-8@SA (about 95% in 24 h), CCM release for 3CCM@ZIF-8@SA and 5CCM@ZIF-8@SA samples were controlled and significantly delayed (about 35% and 27% in 24 h, respectively), and most importantly, the duration of the sustained release of CCM for 5CCM@ZIF-8@SA could reach 72 h or above with a slower releasing rate. As the reason was concerned, 1CCM@ZIF-8@SA released fast possibly because that CCM was mostly eutectic on the surface and would be dissolved rapidly in large amounts upon touching the phosphate buffer solution. On the contrary, most of CCM molecules entered the interior of ZIF-8 for 5CCM@ZIF-8@SA and 3CCM@ZIF-8@SA in addition to the surficial few ones. In particular, CCM in the 5CCM@ZIF-8@SA group fully integrated with the pores in ZIF-8 to achieve the optimal coating rate of the drug, delaying the release rate and prolonging the release time. This conclusion is consistent with the morphologies and structures presented by the SEM images.

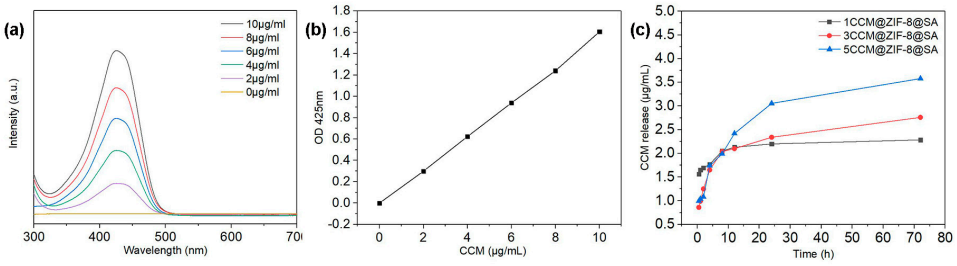

Figure 4. (a) Wavelength scans of ethanol solutions of different CCM concentrations, (b) standard curves of CCM, (c) CCM released from CCM@ZIF-8@SA samples.

2.3. Antibacterial activities of CCM@ZIF-8@SA composite hydrogels

To assess the antibacterial activities of drug-loaded complex hydrogels, we selected gram-positive *Staphylococcus aureus* (*S. aureus*, BNCC186335) and gram-negative *Escherichia coli* (*E. coli*, BNCC336902) for antibacterial assays. Antibacterial performance is assessed by colony forming unit (CFU) assay. After co-incubating the complex hydrogel with bacterial culture medium at 37.5 °C for 24 h, quantitative data (Figure 5a,c) and CFU assay (Figure 5b,d) showed that both the ZIF-8@SA and CCM@ZIF-8@S samples showed good antimicrobial properties against both *S. aureus* and *E. coli*. Among them, the antibacterial efficiency of ZIF-8@SA in *S. aureus* was 28%, and reached 58% in *E. coli*, showing excellent antibacterial effect. The antibacterial efficiencies against *S. aureus* increased to 30%, 42% and 65% for 1/3/5CCM@ZIF-8@SA, respectively, which were 2~4 times higher than that of pure SA (18%). Similar trend was also found in killing *E. coli*, with the values being 70%, 80% and 86% for three samples. ZIF-8@SA performed better than bare SA, possibly because the release of Zn^{2+} from ZIF-8 could cause some damage on the bacteria. This might arise from the disruption of bacterial membrane permeability by Zn^{2+}, which inhibits glycolysis, glucosyltransferase production and polysaccharide synthesis in bacteria[35, 36]. The pleasant antibacterial effects of 1/3/5CCM@ZIF-8@SA hydrogels were thus the synergistic effect of CCM and Zn^{2+}. Based on the coating results of the two types of bacteria and the quantitative analysis of OD values, the OD values followed a decreasing order of SA > ZIF-8@SA > 1CCM@ZIF-8@SA > 3CCM@ZIF-8@SA > 5CCM@ZIF-8@SA both for *E. coli* and *S. aureus*, with 5CCM@ZIF-8@SA performing the best. The good antibacterial properties shown by CCM@ZIF-8@SA finally highlights its practical prospects as wound dressing.

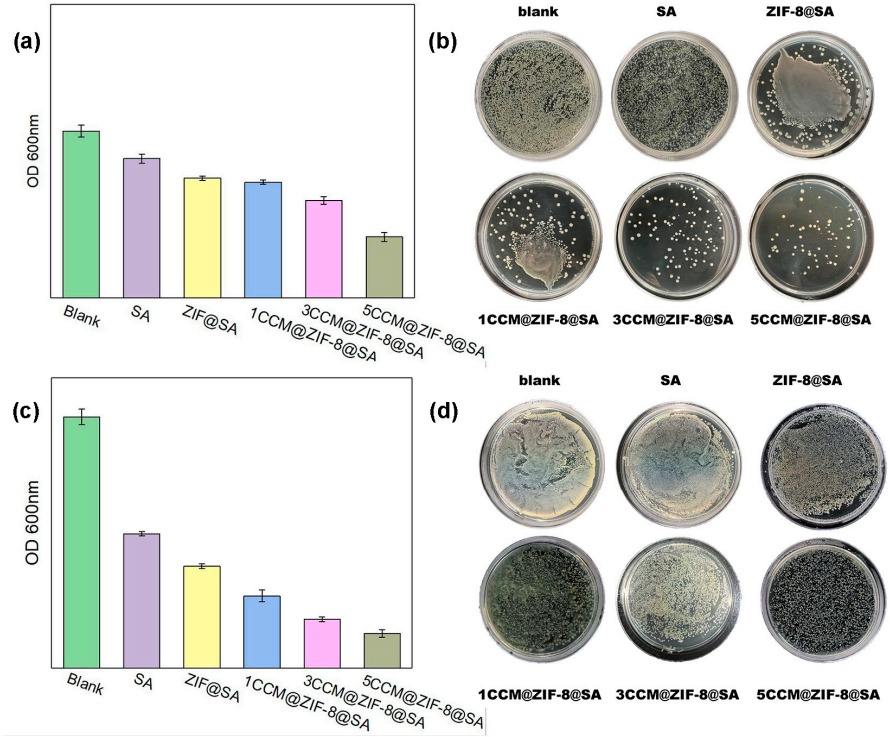

Figure 5. Quantitative measurement of *E. coli* (a), *S. aureus* (c) survival after 24 h of incubation, bacterial inhibition ability of the SA, ZIF-8@SA, 1/3/5CCM@ZIF-8@SA against the clinically established bacterial pathogens [*E. coli* (b) and *S. aureus* (d)].

3. Materials and Methods

3.1. Materials

2-mIM, CCM, SA, zinc chloride, methanol (for synthesis) were purchased from Beijing Bailinway Technology Co., Ltd., phosphate buffer (0.01M) was purchased from Beijing Lanyi Chemical Products Co., Ltd., gram-positive *S. aureus* (BNCC186335) and gram-negative *E. coli* (BNCC336902) were purchased from Beinong Yuhe Technology Development Co., Ltd.

3.2. Synthesis

SA hydrogels were prepared by the ionic cross-linking method. Firstly, the aqueous solution of sodium alginate was prepared by dissolving sodium alginate (30 mg) in H_2O (1 mL) and stirring in a surface dish until homogeneous, and then it was placed in the freezing layer of the refrigerator to make it set. $ZnCl_2$ (545 mg) was dissolved in H_2O (20 mL) and stirred magnetically until the solution was homogeneous. The $ZnCl_2$ solution was added dropwise to the fixed aqueous sodium alginate solution and the reaction was continued for about 2 h to obtain SA hydrogel, and finally the residual $ZnCl_2$ solution was washed with deionized water. Then, CCM@ZIF-8@SA hydrogels were synthesized by co-precipitation of $Zn(NO_3)_2 \cdot 6H_2O$ and 2-mIM in MeOH at room temperature. 2-mIM (330 mg) and CCM (1.0, 3.0 and 5.0 mg) were separately dissolved in MeOH solution (10 mL), and the solution was stirred magnetically until clarified, and then the prepared SA hydrogel was immersed in the above solution and the reaction was continued for 4 h. After the reaction finished, different hydrogels with a ginger yellow solid attached to the surface were obtained, denoted as 1CCM@ZIF-8@SA, 3CCM@ZIF-8@SA and 5CCM@ZIF-8@SA accordingly.

3.3. Characterizations

The topography and microstructure of the hydrogel were observed by the Regulus-8100 cold-field emission scanning electron microscope with an accelerating voltage of 15 kV. Pre-experiment preparation: The hydrogel was made into a 1 cm square, and due to the poor conductivity of the material, in addition to using conductive glue to fix the silicon wafer to the experimental sample stage, pre-spray gold treatment was required. XRD pattern was obtained on the Japanese Rigaku TTR3 X-ray diffractometer, the X-ray source was CuKα target (λ=1.5 Å), the scanning angle of 2θ was 5 °~40 °, and the scanning speed was 10 °/min. Raman scattering spectroscopy was obtained on microconfocal Raman spectrometer (inVia-Reflex), in which the excitation wavelength was 532 nm, the scanning range was 0~1800 cm^{-1}, and the scanning step of 2 cm^{-1} was used to detect the crystal structure of the sample. The Cary 7000 UV-Vis diffuse reflectance spectrometer was used to test the light response range and intensity changes of hydrogel samples with a scanning wavelength of 200-700 nm. The functional groups of the sample were further detected by Fourier infrared spectroscopy (Excalibur 3100 type) in the range of 500-4000 cm^{-1}. The composite hydrogel was stretched by a universal testing machine (TA.HD PLUS) at a speed of 5 mm/min. The maximum stress was divided by the area to obtain the tensile strength.

3.4. Drug release tests

- (i) The standard curve of CCM:
  120 mg of CCM was dissolved in 10 mL of ethanol as the stock solution. Then 1 mL was extracted from the above solution and diluted to give the CCM solution gradients of 10, 8, 6, 4, 2, and 0 μg/mL. Subsequent Measurement of the UV-Vis absorption of these solutions was conducted in the wavelength range of 200-800 nm, and the absorbance intensities at 427 nm were recorded and were plotted as a function of CCM concentrations.
- (ii) The drug release test of CCM@ZIF-8@SA composite hydrogels:
  The as-prepared CCM@ZIF-8@SA composite hydrogel was soaked in 15 mL of phosphate buffer solution (pH=7.4). 3 mL was taken out every time in an interval of 0.5, 1, 2, 4, 8, 24, and 72 h, and the absorbance intensities at 427 nm were measured. Finally, the release amount of CCM was calculated according to the standard curve. In this experiment, three sets of parallel experiments were performed, and the results of the three groups of experiments were averaged and then processed for data processing.

3.5. Antimicrobial properties

- (i) Sample processing:
  The as-prepared hydrogels were put into a centrifuge tube, and were irradiated under ultraviolet lamp for 30 min.
- (ii) Medium configuring:
  4 g of Luria-Bertani (LB) broth was added into 200 mL of deionized water and stirred to obtain liquid medium, and 9.6 g of agar medium was added into 300 mL of deionized water and stirred well to obtain solid medium. Then two different media were put into into the LX-B50L autoclave for sterilization(120 °C, 30 min) and then cooled down. At last, the solid medium was poured into the Petri dish in an ultra-clean stage and stored.
- (iii) Bacterial resuscitation:
  The strains used in this experiment are Gram-positive *S. aureus* (BNCC186335) and Gram-negative *E. coli* (BNCC336902). Before the experiment, 50 mL of centrifugal tube, parafilm and other experimental consumables were subjected to ultraviolet irradiation for 30 minutes on the ultra-clean table for sterilization. During the experiment, a small amount of bacteria was placed in aliquot liquid medium (30 mL) with an overheated inoculation ring, sealed with a breathing membrane, and cultured in a shaker at a temperature of 37 °C for 18 h.
- (IV) Bacterial proliferation:

The bacterial proliferation was analyzed by measuring OD values and coating method. After 24 h of bacterial recovery, removed from the shaker, the bacteria solution was diluted 3-fold by a factor with liquid medium and was measured with a UV spectrophotometer. Under the condition of bacterial concentration of 106 cfu·mL^{-1}, 5 mL of bacterial liquid was extracted and put into a centrifuge tube where the hydrogel samples were added. The bacterial solution was then sealed with a breathing membrane, and put into the incubator at a constant temperature of 37 °C for a total of 24h.

- (V) Determination of bacterial bacteriostatic rate:
  The OD values at 600 nm were measured with the ultraviolet spectrophotometer after diluting the bacterial solution after 24 h of total culture, and then the bacterial solution was diluted by 4 concentration gradients, coated with a plate, and then put into the incubator for culture. The dish was then taken out for colony counting after 24 h to observe the growth of bacteria. The relative bacteriostatic rate was calculated according to the following formula:
  Relative bacteriostatic rate (%) = $\frac{A-B}{A}\times$ 100%
  A - the OD values of the colonies in the blank group;
  B - the OD values of the colonies in the experimental group.

4. Conclusions

In summary, a flexible CCM-loaded Zn-MOF hydrogel was prepared by combining the drug with organic ligands through Zn^{2+} crosslinking and Zn^{2+} centered coordination. The results showed that CCM-loaded ZIF-8 crystals could be homogeneously synthesized onto SA hydrogel, with CCM becoming part of the ZIF-8 ligand. This would strengthen the encapsulation of CCM inside ZIF-8 frameworks for one hand, and meantime enhance the crosslinking by the supplementary intermolecular forces for another hand. As a consequence, flexible and tough composite hydrogel could be obtained to adapt to the mechanical behaviors of human skin. More importantly, long-term drug release could be achieved by this hierarchical structure, and also good antimicrobial properties against *E. coli* and *S. aureus* were obtained. In conclusion, such composite hydrogel promises a wound healing system, which can provide a guideline for future design of practical chronic wound dressings.

Author Contributions: Li J conducted the experiment and processed the data, Fang Q drew some illustrations, Yan Y conceived the work, Chen Y, Li J and Yan Y wrote the paper, and all the authors contributed to the general discussion.

Acknowledgments: This work was financially supported by the National Key R&D Program of China (No. 2021YFB3802200), the Scientific and Technological Innovation Foundation of Shunde Graduate School, USTB (BK22BE012), and international exchange and growth program for young teachers, USTB (QNXM20210017).

References

1. Liu, J. Z.; Dong, J.; Zhang, T.; Peng, Q., Graphene-based nanomaterials and their potentials in advanced drug delivery and cancer therapy. *J Control Release* **2018,** 286, 64-73.
2. Naghdi, T.; Golmohammadi, H.; Vosough, M.; Atashi, M.; Saeedi, I.; Maghsoudi, M. T., Lab-on-nanopaper: An optical sensing bioplatform based on curcumin embedded in bacterial nanocellulose as an albumin assay kit. *Anal. Chim. Acta* **2019,** 1070, 104-111.
3. Fan, Y. T.; Yi, J.; Zhang, Y. Z.; Yokoyama, W., Fabrication of curcumin-loaded bovine serum albumin (BSA)-dextran nanoparticles and the cellular antioxidant activity. *Food Chemistry* **2018,** 239, 1210-1218.
4. Ghosh, S.; Banerjee, S.; Sil, P. C., The beneficial role of curcumin on inflammation; diabetes and neurodegenerative disease: A recent update. *Food Chem. Toxicol* **2015,** 83, 111-124.
5. Zheng, B. J.; McClements, D. J., Formulation of More Efficacious Curcumin Delivery Systems Using Colloid Science: Enhanced Solubility, Stability, and Bioavailability. *Molecules* **2020,** 25, (12), 2791.
6. Wang, X. Y.; Fan, Y. L.; Yan, J. J.; Yang, M., Engineering polyphenol-based polymeric nanoparticles for drug delivery and bioimaging. *Chem. Eng. J* **2022,** 439, 135661.
7. Almawash, S., Solid lipid nanoparticles, an effective carrier for classical antifungal drugs. *Saudi Pharmaceutical Journal* **2023,** 31, (7), 1167-1180.

8. Zhu, H. J.; Li, B. F.; Chan, C. Y.; Ling, B. L. Q.; Tor, J.; Oh, X. Y.; Jiang, W. B.; Ye, E. Y.; Li, Z. B.; Loh, X. J., Advances in Single-component inorganic nanostructures for photoacoustic imaging guided photothermal therapy. *Adv. Drug Deliv. Rev* **2023,** 192, 114644.
9. Pourmadadi, M.; Abbasi, P.; Eshaghi, M. M.; Bakhshi, A.; Manicum, A. L. E.; Rahdar, A.; Pandey, S.; Jadoun, S.; Diez-Pascual, A. M., Curcumin delivery and co-delivery based on nanomaterials as an effective approach for cancer therapy. *J Drug Deliv Sci Technol* **2022,** 78, 103982.
10. Ban, E.; Kim, A., Coacervates: Recent developments as nanostructure delivery platforms for therapeutic biomolecules. *Int J Pharm* **2022,** 624, 122058.
11. Hirschbiegel, C. M.; Zhang, X.; Huang, R.; Cicek, Y. A.; Fedeli, S.; Rotello, V. M., Inorganic nanoparticles as scaffolds for bioorthogonal catalysts. *Adv Drug Deliv Rev* **2023,** 195, 114730.
12. Jang, E. H.; Kim, G. L.; Park, M. G.; Shim, M. K.; Kim, J.-H., Hypoxia-responsive, organic-inorganic hybrid mesoporous silica nanoparticles for triggered drug release. *Journal of Drug Delivery Science and Technology* **2020,** 56.
13. Mohan, B.; Kamboj, A.; Virender; Singh, K.; Priyanka; Singh, G.; Pombeiro, A. J. L.; Ren, P., Metal-organic frameworks (MOFs) materials for pesticides, heavy metals, and drugs removal: Environmental safety. *Separation and Purification Technology* **2023,** 310.
14. Acharya, A. P.; Sezginel, K. B.; Gideon, H. P.; Greene, A. C.; Lawson, H. D.; Inamdar, S.; Tang, Y.; Fraser, A. J.; Patel, K. V.; Liu, C.; Rosi, N. L.; Chan, S. Y.; Flynn, J. L.; Wilmer, C. E.; Little, S. R., In silico identification and synthesis of a multi-drug loaded MOF for treating tuberculosis. *J Control Release* **2022,** 352, 242-255.
15. Gupta, A.; Keddie, D. J.; Kannappan, V.; Gibson, H.; Khalil, I. R.; Kowalczuk, M.; Martin, C.; Shuai, X.; Radecka, I., Production and characterisation of bacterial cellulose hydrogels loaded with curcumin encapsulated in cyclodextrins as wound dressings. *Eur. Polym. J* **2019,** 118, 437-450.
16. Norahan, M. H.; Pedroza-Gonz, S. C.; Sanchez-Salazar, M. G.; Alvarez, M. M.; Santiago, G. T. D., Structural and biological engineering of 3D hydrogels for wound healing. *Bioact. Mater* **2023,** 24, 197-235.
17. Liu, K.; Chen, Y. Y.; Zha, X. Q.; Li, Q. M.; Pan, L. H.; Luo, J. P., Research progress on polysaccharide/protein hydrogels: Preparation method, functional property and application as delivery systems for bioactive ingredients. *Food Res. Int* **2021,** 147, 110542.
18. Li, H. B.; Cheng, F.; Wei, X. J.; Yi, X. T.; Tang, S. Z.; Wang, Z. Y.; Zhang, Y. S.; He, J. M.; Huang, Y. D., Injectable, self-healing, antibacterial, and hemostatic N,O-carboxymethyl chitosan/oxidized chondroitin sulfate composite hydrogel for wound dressing. *Mater. Sci. Eng. C* **2021,** 118, 111324.
19. Zhang, X. J.; Lin, G.; Kumar, S. R.; Mark, J. E., Hydrogels prepared from polysiloxane chains by end linking them with trifunctional silanes containing hydrophilic groups. *Polymer* **2009,** 50, (23), 5414-5421.
20. Badsha, M. A. H.; Khan, M.; Wu, B. L.; Kumar, A.; Lo, I. M. C., Role of surface functional groups of hydrogels in metal adsorption: From performance to mechanism. *J. Hazard. Mater* **2021,** 408, 124463.
21. Gutiérrez, M.; Ferrer, M. L.; Mateo, C. R.; Monte, F. D., Freeze-drying of aqueous solutions of deep eutectic solvents: a suitable approach to deep eutectic suspensions of self-assembled structures. *Langmuir* **2009,** 25, (10), 5509-5515.
22. Su, H.; Sun, F.; Jia, J.; He, H.; Wang, A.; Zhu, G., A highly porous medical metal-organic framework constructed from bioactive curcumin. *Chem Commun (Camb)* **2015,** 51, (26), 5774-7.
23. Wu, C. S.; Xiong, Z. H.; Li, C.; Zhang, J. M., Zeolitic imidazolate metal organic framework ZIF-8 with ultra-high adsorption capacity bound tetracycline in aqueous solution. *RSC Adv* **2015,** 5, (100), 82127-82137.
24. Devarayapalli, K. C.; Vattikuti, S. V. P.; Yoo, K. S.; Nagajyothi, P. C.; Shim, J., Rapid microwave-assisted construction of ZIF-8 derived ZnO and ZnO@Ta2O5 nanocomposite as an efficient electrode for methanol and urea electro-oxidation. *J. Electroanal. Chem* **2020,** 878, 114634.
25. Geng, C.; Liu, X.; Ma, J.; Ban, H.; Bian, H.; Huang, G., High strength, controlled release of curcumin-loaded ZIF-8/chitosan/zein film with excellence gas barrier and antibacterial activity for litchi preservation. *Carbohydr Polym* **2023,** 306, 120612.
26. Moussawi, R. N.; Patra, D., Modification of nanostructured ZnO surfaces with curcumin: fluorescence-based sensing for arsenic and improving arsenic removal by ZnO. *RSC Adv* **2016,** 6, (21), 17256-17268.
27. Kurkcuoglu, G. S.; Kavlak, I.; Kinik, B.; Sahin, O., Experimental and theoretical studies on the molecular structures and vibrational spectra of cyanide complexes with 1,2-dimethylimidazole: M(dmi)(2)Ni(mu-CN)(4) (M = Cu, Zn or Cd). *J. Mol. Struct* **2020,** 1199, 126892.
28. Kumari, G.; Jayaramulu, K.; Maji, T. K.; Narayana, C., Temperature Induced Structural Transformations and Gas Adsorption in the Zeolitic Imidazolate Framework ZIF-8: A Raman Study. *Journal of Physical Chemistry A* **2013,** 117, (43), 11006-11012.
29. Radhakrishnan, D.; Narayana, C., Guest dependent Brillouin and Raman scattering studies of zeolitic imidazolate framework-8 (ZIF-8) under external pressure. *J. Chem. Phys* **2016,** 144, (13), 134704.
30. Zheng, M.; Liu, S.; Guan, X. G.; Xie, Z. G., One-Step Synthesis of Nanoscale Zeolitic Imidazolate Frameworks with High Curcumin Loading for Treatment of Cervical Cancer. *ACS Appl. Mater. Interfaces* **2015,** 7, (40), 22181-22187.

31. Wang, H.; Lu, Z.; Wang, F.; Li, Y.; Ou, Z.; Jiang, J., A novel strategy to reinforce double network hydrogels with enhanced mechanical strength and swelling ratio by nano cement hydrates. *Polymer* **2023,** 269.
32. Xu, P.; Shang, Z.; Yao, M.; Li, X., Mechanistic insight into improving strength and stability of hydrogels via nano-silica. *Journal of Molecular Liquids* **2022,** 357.
33. Nikpour, S.; Ansari-Asl, Z.; Sedaghat, T.; Hoveizi, E., Curcumin-loaded Fe-MOF/PDMS porous scaffold: Fabrication, characterization, and biocompatibility assessment. *Journal of Industrial and Engineering Chemistry* **2022,** 110, 188-197.
34. Kang, L.; Liang, Q.; Abdul, Q.; Rashid, A.; Ren, X.; Ma, H., Preparation technology and preservation mechanism of gamma-CD-MOFs biaological packaging film loaded with curcumin. *Food Chem* **2023,** 420, 136142.
35. Phan, T. N.; Buckner, T.; Sheng, J.; Baldeck, J. D.; Marquis, R. E., Physiologic actions of zinc related to inhibition of acid and alkali production by oral streptococci in suspensions and biofilms. *Oral Microbiology and Immunology* **2010,** 19, (1), 31-38.
36. Liu, Z.; Tan, L.; Liu, X.; Liang, Y.; Zheng, Y.; Yeung, K. W. K.; Cui, Z.; Zhu, S.; Li, Z.; Wu, S., Zn(2+)-assisted photothermal therapy for rapid bacteria-killing using biodegradable humic acid encapsulated MOFs. *Colloids Surf B Biointerfaces* **2020,** 188, 110781.